A Study of Heat-Affected Zone Cracking in Fe-Containing Ni_3Al Alloys

Grain boundary weakness at elevated temperatures is responsible for the observed cracking in the heat-affected zone

BY M. L. SANTELLA AND S. A. DAVID

ABSTRACT. A key issue in the development of Ni_3Al alloys for engineering applications is weldability. The alloys used for this study were Ni_3Al containing 10 at.-% Fe and either 200 or 500 ppm (weight) B. Weldability was evaluated by making full-penetration electron beam welds on thin sheet. Examination of the weldments showed that heat-affected zone (HAZ) cracking occurred only in the 500 ppm B alloy (IC-25) at welding speeds above 13 mm/s (0.51 in./s). Analysis of weldment microstructures suggested that a weakening of grain boundaries at high temperatures caused the HAZ cracking. Gleeble testing was used to study the hot ductility of the Ni-Fe aluminides in the temperature range of 600°-1300°C (1112°-2370°F) at a strain rate of 3.2 s^{-1}. The results showed that these alloys have poor high-temperature ductility and indicated that the grain-boundary strength of the 200 ppm B alloy (IC-103) was higher at elevated temperatures than that of the 500 ppm B alloy. Therefore, both the weldability evaluation and the hot ductility testing agreed on the effect of boron, and they suggested that low grain-boundary strength at elevated temperature resulted in HAZ cracking during welding.

Introduction

The nickel aluminide Ni_3Al is an ordered intermetallic compound having the $L1_2$ face-centered-cubic (FCC) crystal structure below about 1395°C (2543°F) (Ref. 1). It has many unique properties, such as yield strength that increases with temperature. Unlike many other intermetallic compounds, Ni_3Al exists over a relatively large range of composition, being stable from about 72 to 78.5 at.-% Ni at temperatures below 1150°C (2102°F) (Refs. 1, 2). This range of stoichiometry means that Ni_3Al may be extensively alloyed. For instance, many of the basic properties of Ni_3Al can be maintained at levels as high as 13 at.-% of ternary elements, *e.g.*, Co, Cu, Fe, Ti and V (Refs. 3, 4). The strong tendency for long-range order in Ni_3Al and its alloys means that atomic mobility is somewhat restricted. Thus, Ni_3Al is resistant to diffusion-controlled processes, and its structural stability at high temperatures is very good. These aluminides also tend to form adherent aluminum oxide scales. This characteristic, along with low atomic mobility in the base metal, provides good resistance to oxidation and corrosion at high temperatures (Refs. 5, 6). Lastly, the fact that the Ni_3Al alloys have an FCC crystal structure means that enough slip systems are available to permit extensive plastic deformation of polycrystals (Ref. 7).

The combination of properties displayed by Ni_3Al alloys would seem to make these materials strong candidates for use in a wide variety of structural applications. However, a major impediment to the use of Ni_3Al as an engineering material has been its brittleness in polycrystalline form. Although it has been known for years that single crystals of Ni_3Al can exhibit good ductility (Refs. 8-10), polycrystals were known to be brittle (Refs. 8, 11-13). The low ductility of polycrystalline Ni_3Al results from grain boundary weakness, which causes fracture to occur intergranularly with little or no deformation within individual grains. The exact cause of this behavior is not known (Refs. 14, 15). More importantly, the brittle behavior of Ni_3Al has precluded its use for structural components because of its lack of fabricability and fear of catastrophic failure.

In recent times, Aoki and Izumi (Ref. 16) found that boron additions could have a substantial beneficial effect on the ductility of polycrystalline Ni_3Al, and C. T. Liu and co-workers at Oak Ridge National Laboratory (Refs. 17-19) have begun developing a series of ductile, polycrystalline, Ni_3Al alloys. The approach in these latter studies (Refs. 17-19) has been to use a combination of macroalloying and microalloying to control the mechanical and metallurgical behavior of Ni_3Al. Macroalloying involves alloy additions of many percent to the base Ni_3Al compound and is used to control phase stability and bulk properties. Microalloying involves the addition of small amounts (usually ppm) of selected elements to control the chemistry of grain boundaries (Refs. 20, 21). Microalloying with boron can alleviate brittle intergranular fracture in Ni_3Al and its alloys (Refs. 17, 18, 22). Some of the more promising alloys, at present, are based on the Ni_3Al-Fe_3Al pseudo-binary system. Iron dissolves in Ni_3Al up to about 13 at.-% without disturbing the $L1_2$ crystal structure or causing the stabilization of second phases at low temperatures. Iron also appears to improve the metallurgical properties of Ni_3Al alloys, and because iron is cheaper than nickel, substitution of iron into Ni_3Al reduces overall alloy cost. Those considerations are important commercially.

Besides the considerations already mentioned, weldability has become a key issue in the development of these new Ni_3Al-based alloys because joining by conventional welding processes is an important means of fabricating engineering alloys into structural components. This paper outlines a study which shows that defect-free, full-penetration, autogenous welds can be made in Ni_3Al alloy sheet containing 10 at.-% iron. However, cracking problems do exist, with the heat-affected zone (HAZ) being the most likely location for this type of defect. A study of welding behavior has shown that both alloy composition and welding

Paper presented at the 66th AWS Annual Convention held in Las Vegas, Nev., April 29-May 3, 1985.

M. L. SANTELLA is a Research Staff Member and S. A. DAVID is Group Leader, Materials Joining Group, Metals and Ceramics Division, Oak Ridge National Laboratory, Oak Ridge, Tenn.

speed affect the susceptibility to HAZ cracking. Also presented in this paper are the results of hot ductility tests, performed on the iron-containing Ni_3Al, which show that boron content affects the high-temperature ductility of these alloys. The hot ductility results are discussed in detail with respect to microstructure and are correlated to the weldability observations.

Experimental Details

The nominal compositions of the Fe-containing Ni_3Al alloys, IC-25 (500 ppm B) and IC-103 (200 ppm B), used in this study are listed in Table 1. Ingots (500 g) of the alloys were prepared from pure charge materials and a Ni-18 at.-% B master alloy by vacuum arc melting and drop casting. The 125 × 25 × 9 mm (5 × 1 × 0.35 in.) ingots were processed into 0.7 mm (0.03 in.) thick sheet by cold rolling. After the final annealing treatment, the alloys had a recrystallized grain size of ASTM 8-9 (15-20 μm); they were also single phase and fully ordered. A cross-section through the ternary phase diagram for these alloys is shown in Fig. 1. The equilibrium solid phases are identified as follows: γ is disordered FCC, γ' is ordered FCC ($L1_2$), and β is ordered BCC (B2). A nonequilibrium phase that also occurs in this system is termed β', and it appears to form from the β phase as a result of rapid cooling (Refs. 18, 23).

Autogenous bead-on-plate weldments were made by electron beam (EB) welding. The welding variables were adjusted to produce full-penetration welds at various travel speeds. The welds were made in a 6 kW machine with the beam focal spot set for the sheet surface. The welding speed varied from 0.9 to 64 mm/s (0.03 to 2.5 in.). Electron beam voltages were 60 to 100 kV, and beam currents were 1 to 6 mA. All welds were made on 20 × 40 × 0.7 mm (0.8 × 1.6 × 0.03 in.) coupons of annealed aluminide sheet. Before welding, each coupon was lightly polished to remove surface oxide and cleaned with acetone. The coupons were positioned for welding in order to minimize restraint. Weld beads were typically 2 to 3 mm (0.08 to 0.12 in.) wide and 35 to 40 mm (1.4 to 1.6 in.) long. Both upper and lower as-welded surfaces were examined for cracks at a magnification of 100×.

Hot ductility testing was done on a Gleeble 1500 thermomechanical simulator. Because the availability of these alloys was limited, and they were typically in sheet form, subsize specimens (Fig. 2) were used for the hot ductility tests. The specimens were held in pinned, copper, crosshead pieces, which were placed in the standard copper chucks normally used for 6.35 mm (0.25 in.) diameter bars. Once a test procedure was established, specimens could be subjected to a HAZ thermal cycle with excellent control. The thermal cycle used is shown in Fig. 3. It was measured in the HAZ of an EB weld on 0.7 mm (0.03 in.) sheet. The peak temperature of the thermal cycle was 1325°C (2417°F), and it corresponds to a point very near the fusion line of the welds made in these

Table 1—Alloy Compositions, in Atomic Percent

Alloy Identification	Composition Ni	Al	Fe	B	Others
IC-25	69.9	18.9	10.0	0.24 (500 ppm-wt.)	0.5 Ti + 0.5 Mn
IC-103	70.0	18.9	10.0	0.10 (200 ppm-wt.)	0.5 Ti + 0.5 Mn

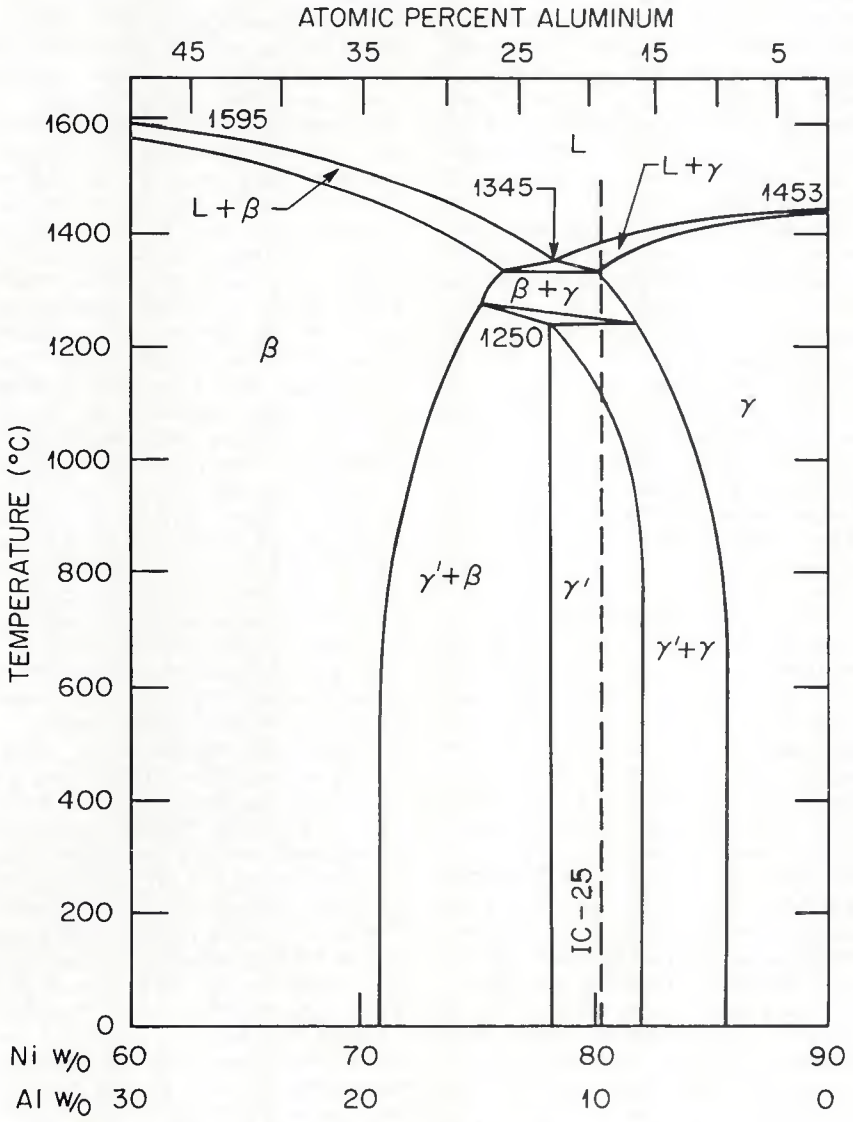

Fig. 1—Vertical section of Ni-Al-Fe system at 10 wt.-% (approximately 10 at.-%) Fe

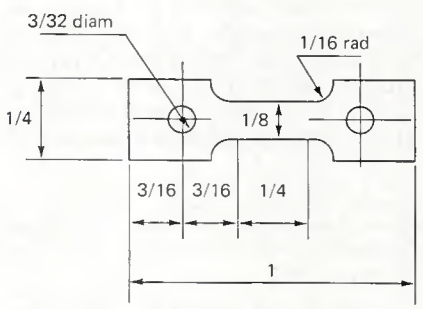

DIMENSIONS IN INCHES.
SPECIMEN THICKNESS ≅ 0.028 in. (0.7 mm)

Fig. 2—Schematic of subsize specimens used for hot ductility testing

alloys. The ductility tests were performed at temperatures of 600° to 1300°C (1112° to 2372°F) on both the heating and cooling portion of the thermal cycle. Figure 3 indicates the location of the test conditions, as well as the phases present (at equilibrium) for each. Specimen temperature was monitored by a single thermocouple attached in the middle of the 6.35 mm (0.25 in.) gauge length. Independent measurements indicated that no significant thermal gradients developed within the gauge length. All tests were run in air. The reported ductility values represent percent elongation within the gauge length.

Weldment specimens were examined by optical and electron metallographic techniques. For scanning electron microscopy (SEM), welds were notched and fractured transverse to the welding direction. The resulting fracture surfaces permitted examination of fusion zone (FZ), HAZ, and base metal on one specimen. Full details of all metallographic techniques have been presented elsewhere (Refs. 18, 23).

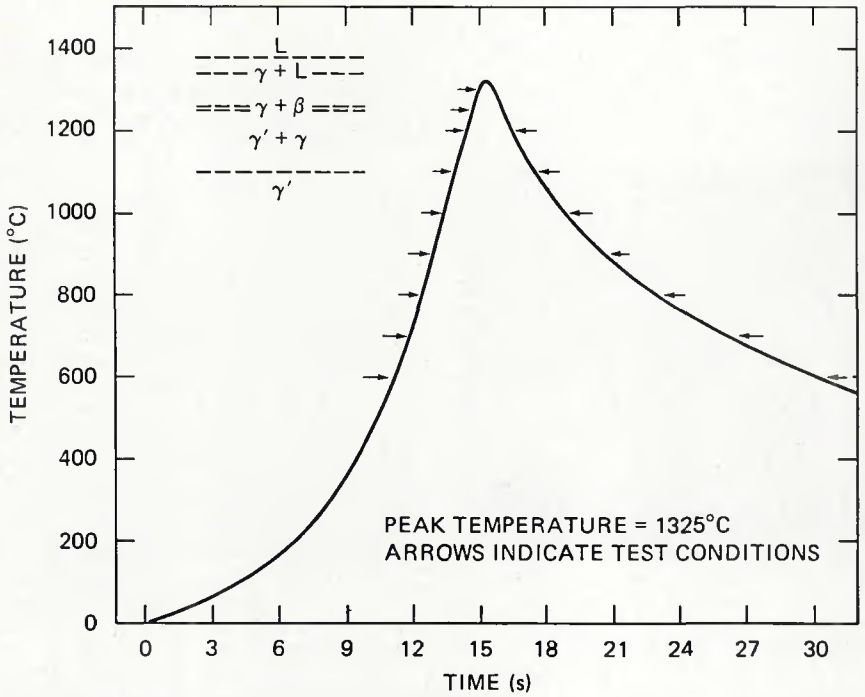

Fig. 3—Thermal cycle used for hot ductility tests

Results

Weldability of Fe-Containing Ni_3Al

Alloy IC-25 was EB welded at speeds ranging from 0.9 to 64.0 mm/s (0.04 to 2.5 in./s); alloy IC-103 was EB welded at speeds ranging from 0.9 to 50.8 mm/s (0.04 to 2.0 in./s). Cracking frequency has been plotted versus welding speed for those tests, along with some data of David, *et al.* (Ref. 23), in Fig. 4. These results confirmed that IC-25 weldments were very susceptible to cracking at welding speeds exceeding about 13 mm/s (0.5 in./s). On the other hand, sound, crack-free welds were made in IC-103 at speeds up to 50.8 mm/s (2 in./s). Figure 5 shows a weldment microstructure for IC-25. Although occasional FZ cracks were observed in IC-25, most were confined to the HAZ. All crack paths were intergranular, and HAZ cracks tended to extend in a direction normal to the welding direction.

The fusion zones in both alloys were

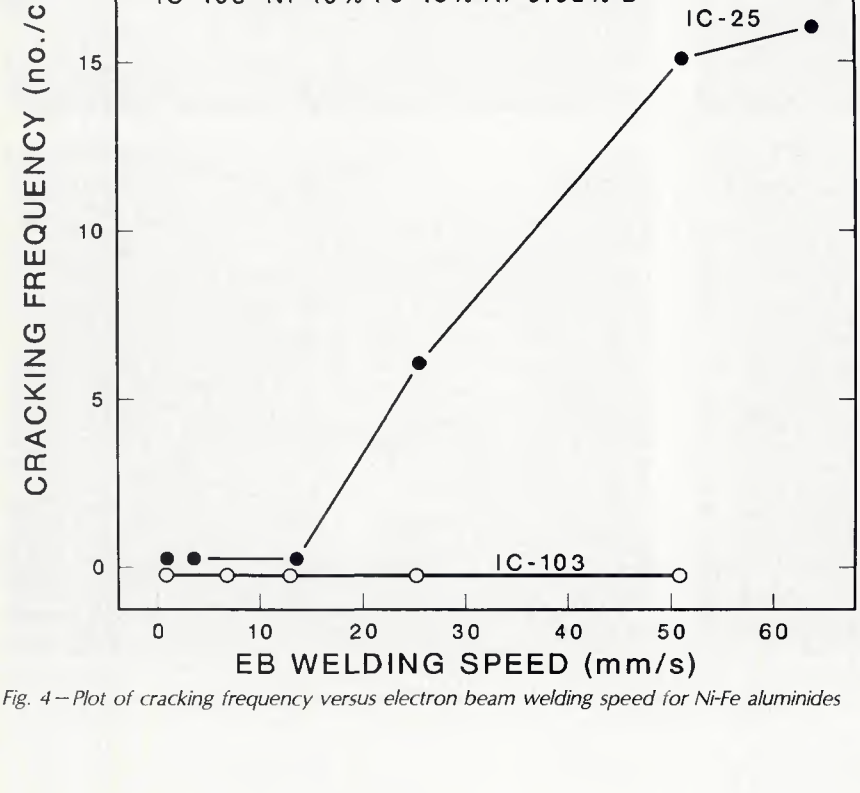

Fig. 4—Plot of cracking frequency versus electron beam welding speed for Ni-Fe aluminides

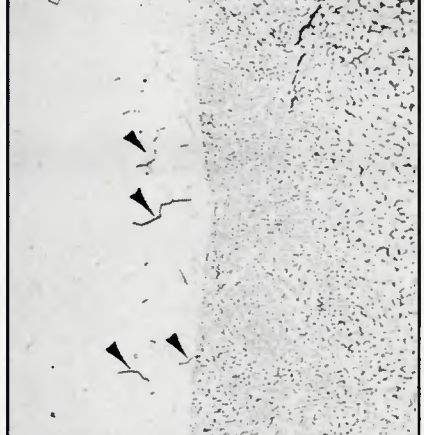

Fig. 5—Microstructure of IC-25 sample, electron beam welded at 64 mm/s, viewed from weldment surface

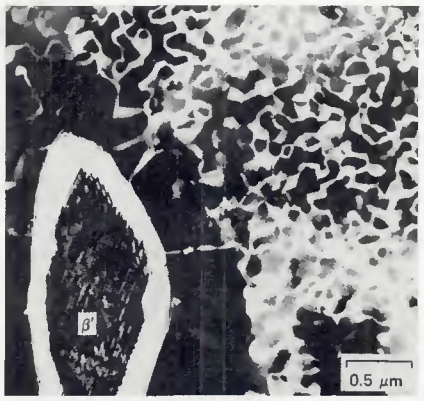

Fig. 6 — Transmission electron micrograph showing fusion zone microstructure. The matrix phase is ordered γ′. The second phase is β′

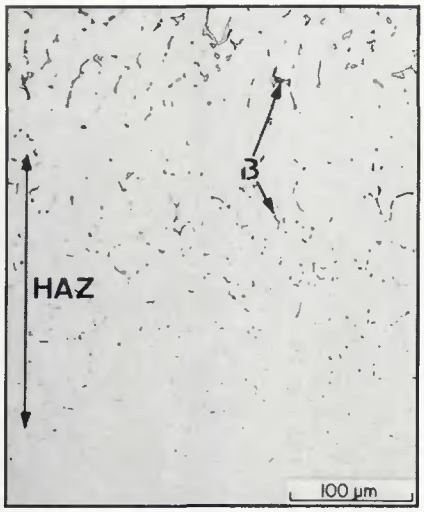

Fig. 7 — Typical microstructure of low-speed electron beam weld viewed from weldment surface. HAZ grain boundaries are decorated with β′ phase

two-phased, with the primary phase being the ordered γ' solid solution. The second phase, distributed interdendritically, appeared to be martensitic, and is termed β' phase. The exact crystal structure of this microconstituent is not known, but available data indicate it may be ordered body-centered-tetragonal (Ref. 23). The β' phase in Ni-Fe aluminides apparently forms from aluminum-rich β phase (Ref. 23), and its general nature suggests that it is similar to a martensitic phase which forms from the β phase in the Ni-Al binary system (Refs. 24, 25). A typical FZ microstructure, as observed in the transmission electron microscope, is shown in Fig. 6. The volume fraction of second phase in the fusion zone was determined by point counting; it varied from 0.09 to 0.12, increasing with welding speed. The β' phase also formed on the HAZ grain boundaries in both alloys (Fig. 7), particularly at welding speeds below about 13 mm/s. The extent of HAZ β' formation increased with

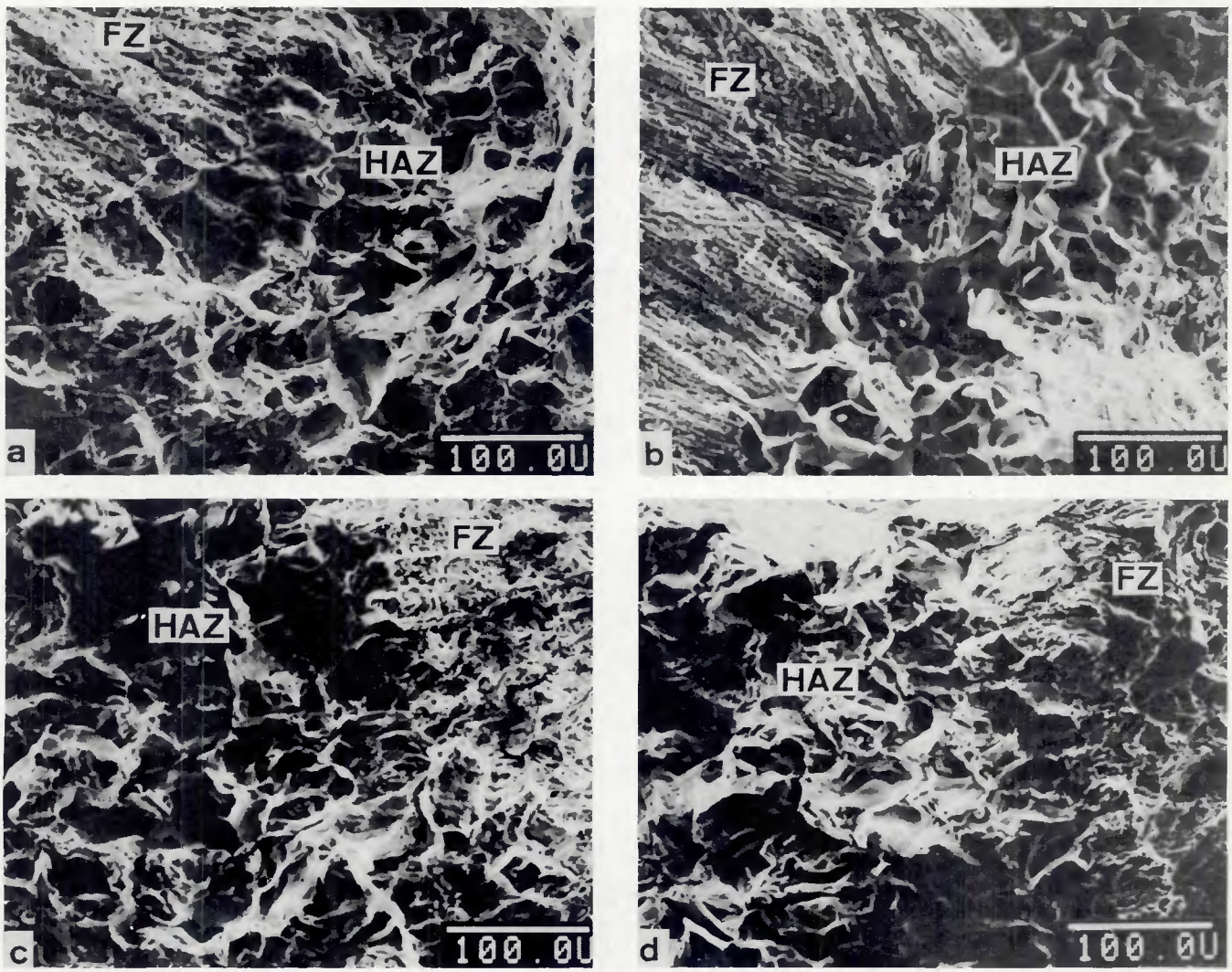

Fig. 8 — Scanning electron micrographs of fracture surfaces showing cross-sectional view of electron beam weldment microstructures. A — IC-25 welded at 4.2 mm/s. B — IC-25 welded at 33.9 mm/s. C — IC-103 welded at 4.2 mm/s. D — IC-103 welded at 33.9 mm/s

decreasing speed. Optical metallography failed to reveal any apparent difference in the details of weldment microstructure between IC-25 and IC-103, other than the absence of cracks in IC-103.

To examine the effect of welding speed on HAZ microstructure in more detail, coupons of IC-25 and IC-103 welded at 4.2 and 33.9 mm/s (0.16 and 1.33 in./s) were fractured at room temperature by loading parallel to the weld axis. The exposed fracture surfaces (Fig. 8) correspond to cross-sectional views of each of the four weldments. On each fracture surface, three distinct regions were visible: FZ, HAZ and base metal. Solidification structure was apparent in the FZ, and the base metal showed the ductile transgranular failure mode typical of Ni_3Al fractured at room temperature (Ref. 22). Differences in microstructure, however, existed for these weldments in the HAZ regions. Figures 8A and 8C, respectively, show the low-speed HAZ microstructure for IC-25 and IC-103. In both cases, the fracture mode is mixed, but with more of an intergranular nature than unaffected base metal. Furthermore, IC-25 shows more ductile tearing than IC-103 (Fig. 9), which is consistent with the effect of boron on ductility and fracture of the base metals at room temperature. The higher boron level alloys (500–1000 ppm) generally have better room-temperature ductility than those with boron levels in the 200 ppm range (Refs. 17, 18, 22). Also, the fusion line in the low-speed welds was not distinct because of significant β' formation on the HAZ grain boundaries. A more dramatic difference between IC-25 and IC-103 was seen in the high speed HAZ microstructures. In this case, the microstructure of IC-103 (Fig. 8D) was very similar to that observed in the HAZ of the low-speed weld. However, IC-25 (Fig. 8B) showed brittle intergranular fracture in the HAZ. Close inspection of the HAZ's of both alloys revealed their fusion lines to be very distinct, compared with those of the low-speed welds. Also, the HAZ grain boundaries were largely free of any second phases. Careful examination of this IC-25 specimen indicated that it broke across pre-existing HAZ cracks. There was no evidence of liquid films on the IC-25 crack surface, indicating that this HAZ crack occurred after passage of the molten weld pool, *i.e.*, at some temperature below the solidus.

Hot Ductility Testing of Fe-Containing Ni_3Al

The tensile ductility of IC-25 as a function of temperature is shown in Fig. 10. The bottom part of Fig. 10 shows the behavior for tests conducted on the heating portion of the HAZ thermal cycle (on-heating specimens). The ductility of IC-25 decreased from 18.8% at 600°C (1112°F) to near zero at 800°C (1472°F), and there was no recovery of ductility as the test temperature was increased. The results from tests conducted on the cooling portion of the thermal cycle (on-cooling specimens) are given in the top part of Fig. 10. In this case, no significant ductility was measured above 600°C. At 600°C, the IC-25 specimen tested on cooling had a ductility of 8.9%.

The tensile ductility data of IC-103 are shown in Fig. 11. The general trend of these results is similar to that observed for IC-25, with one notable exception.

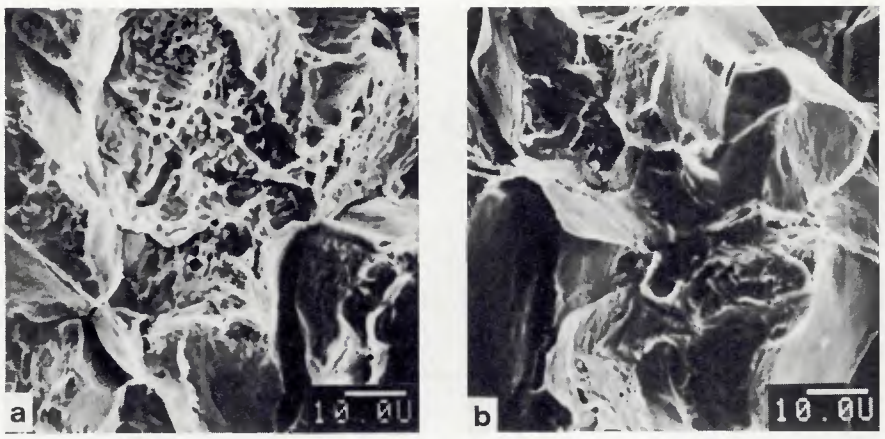

Fig. 9—Scanning electron micrographs of heat-affected zone microstructure for low-speed welds in A—IC-25 and B—IC-103.

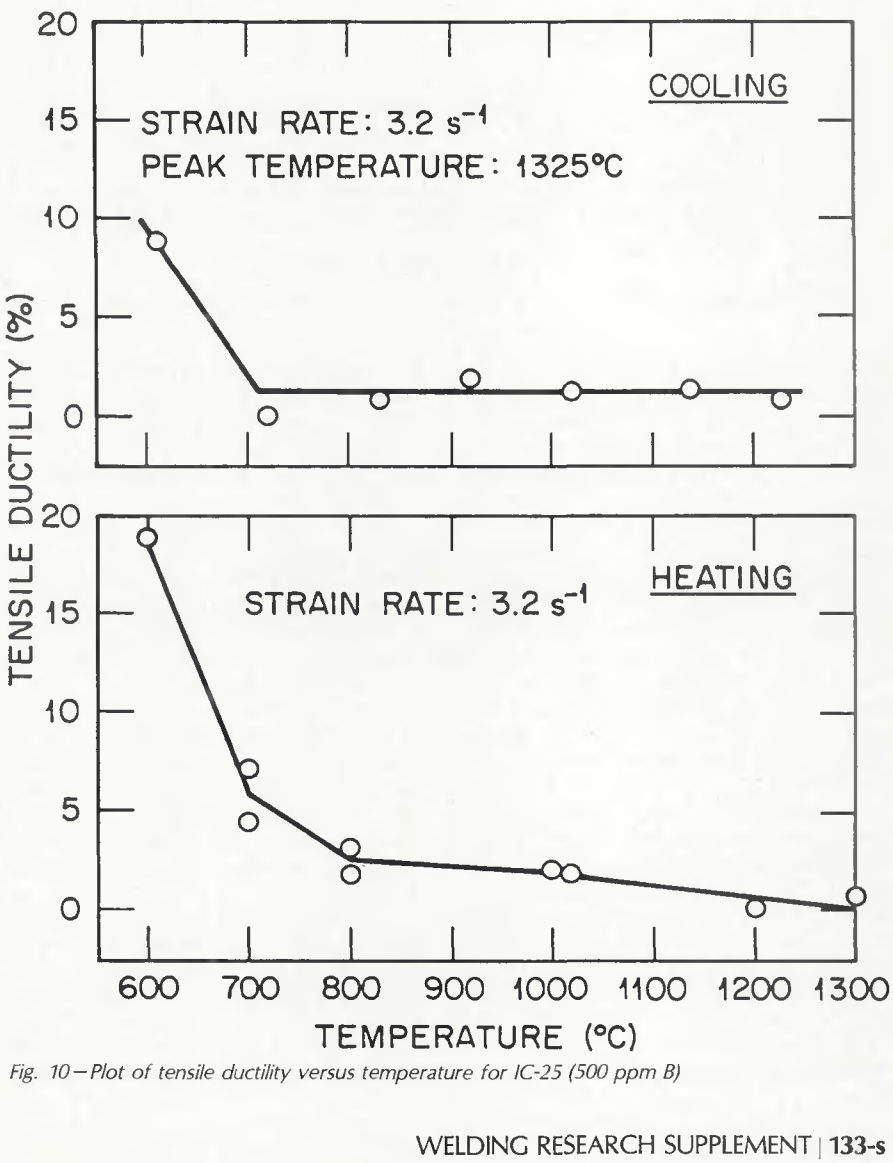

Fig. 10—Plot of tensile ductility versus temperature for IC-25 (500 ppm B)

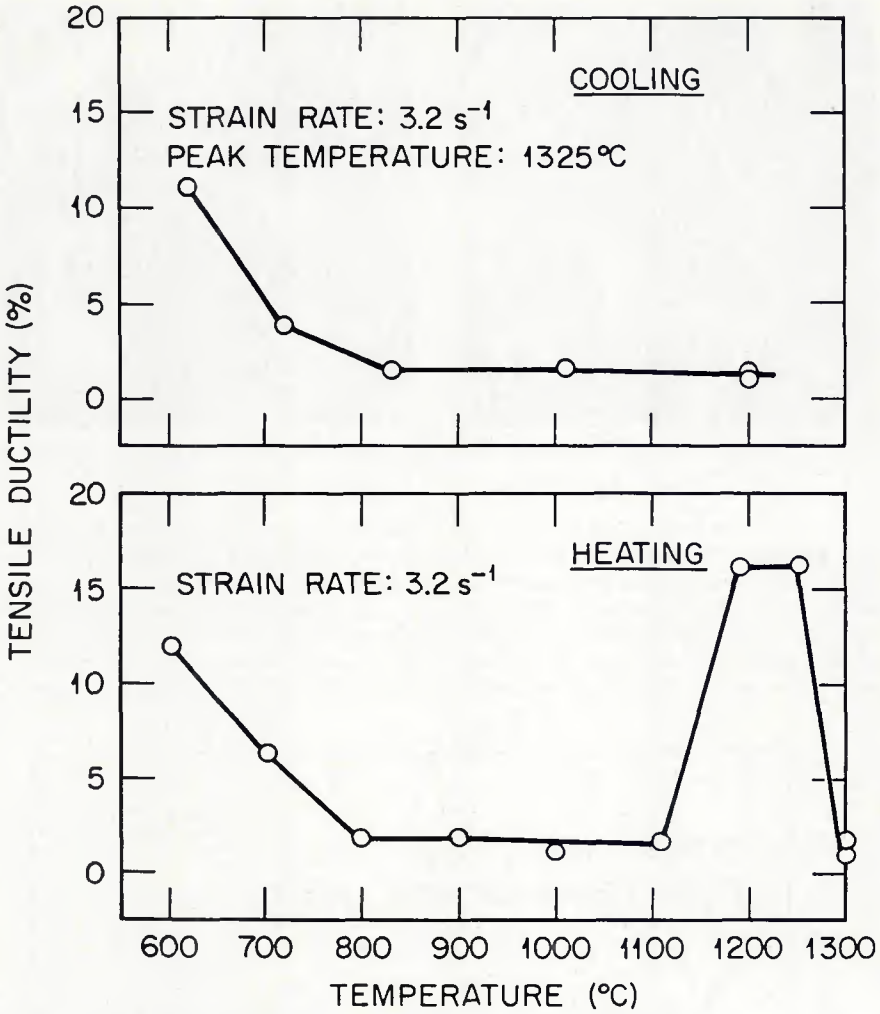

Fig. 11—Plot of tensile ductility versus temperature for IC-103 (200 ppm B)

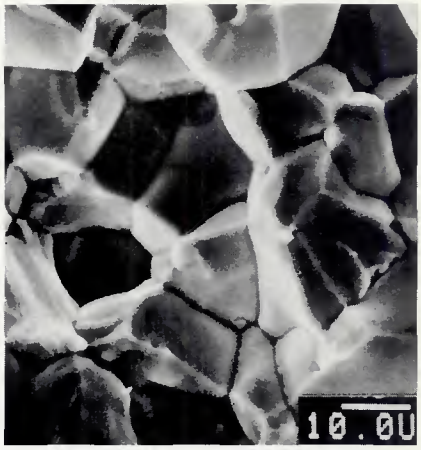

Fig. 12—Fracture appearance of IC-25 tested at 1200°C on heating. Elongation = 0%

Fig. 13—Fracture appearance of IC-25 tested at 1000°C on cooling. Elongation = 0%

For on-heating tests conducted in the temperature range of 1200° to 1250°C (2192° to 2282°F), IC-103 exhibited ductility values slightly in excess of 16%. The ductility of specimens tested on the cooling portion of the thermal cycle is given in the top portion of Fig. 11. Where a ductility value of 16.1% was measured for the on-heating specimen at 1200°C, no ductility was observed at this temperature for tests conducted on cooling. The ductility of on-cooling specimens began to recover below 800°C (1472°F), with the on-cooling ductility values at 600° and 700°C (1112° and 1292°F) being slightly lower than the corresponding on-heating values.

A combination of optical and scanning electron microscopy was used to characterize the fracture behavior of these two alloys. The fracture appearance of IC-25 tested at 1200°C on heating is shown in Fig. 12. This specimen exhibited complete intergranular failure. The small amount of ductility measured in this case was most likely the result of secondary cracks and of measurement errors (which may overestimate the elongation by about one percent). This fracture appearance is consistent with brittle behavior, and it was typical of those specimens of IC-25 and IC-103 that were tested on heating at 800° to 1250°C and exhibited little measurable ductility.

The fracture appearance of IC-25 tested at 1000°C (1832°F) on the cooling portion of the HAZ thermal cycle is shown in Fig. 13. In this case, films of the β phase have formed on the grain boundaries, somewhat complicating the microstructure. Nevertheless, a distinct intergranular nature existed on this surface. All the specimens of both alloys tested at 800°C and above on cooling had fracture surfaces similar in appearance to that shown in Fig. 13. Typically, these specimens had evidence of some secondary cracking but no significant ductility.

The data points that stand out among those plotted in Figs. 10 and 11 are the ones for IC-103 tested on heating at 1200° and 1250°C. These two specimens had ductility values of 16.1 and 16.2%, respectively, and both had a large reduction of area, although this property was not estimated. The fracture appearance of IC-103 tested on heating at 1200°C is presented in Fig. 14. This surface has an intergranular nature overall, but it indicates that the grains have undergone large deformations before fracture. The grain boundaries appear to have separated by ductile tearing, and their appearance suggests that local recrystallization may have occurred. Optical metallography confirmed these observations, showing that grains near the fracture plane had indeed deformed considerably and that the grain boundaries were saturated with very small recrystallized grains. Figure 15 shows the fracture surface of IC-103 tested at 1250°C. The structure shown in this SEM micrograph indicates that the failure mode at this temperature is transgranular. The details of the fracture surface suggest that ductile tearing may have occurred, followed by or simultaneous with recrystallization. The transgranular nature of fracture at 1250°C was confirmed by optical metallography. Examination of the optical microstructure also indicated that this tensile specimen had undergone

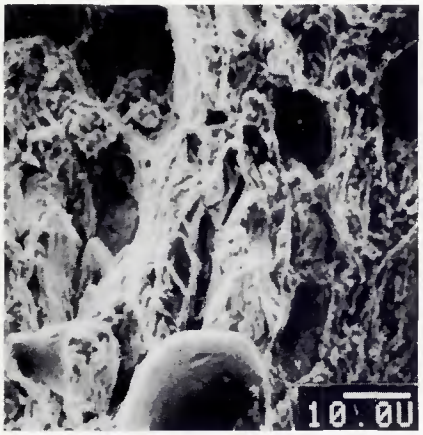

Fig. 14 – Fracture appearance of IC-103 tested at 1200°C on heating. Elongation = 16.1%

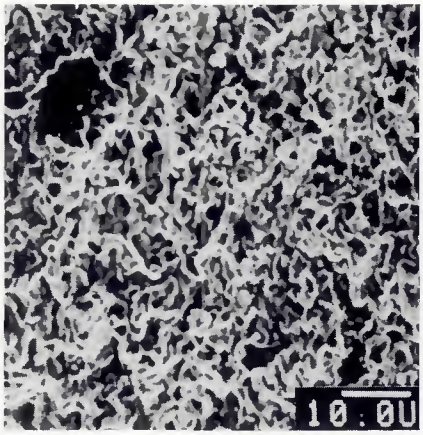

Fig. 15 – Fracture appearance of IC-103 tested at 1250°C on heating. Elongation = 16.2%

Fig. 16 – Fracture appearance of IC-103 tested at 1300°C on heating. Elongation = 0%

complete recrystallization and had no sign of β phase formation. Alloy IC-25 was not tested at 1250°C on heating, but a comparison between IC-25 and IC-103 at 1200°C is presented in Table 2.

The highest temperature used for ductility testing of IC-25 and IC-103 was 1300°C (2372°F), and these tests were done only on heating. The fracture surface of IC-103 shown in Fig. 16 was typical of both alloys. The failure mode was completely intergranular, but the grain edges were not as distinct at this temperature as they were on specimens showing brittle fracture at lower temperatures. Also, there is evidence of second phase formation on some boundaries, and this was confirmed by optical examination. Neither alloy displayed any ductility at 1300°C.

Discussion

The compositions of IC-25 and IC-103 were chosen on the basis of previous work, which showed that both iron and boron can affect the welding behavior of Ni_3Al. Iron additions of 10 at.-% have been shown to improve the weldability of Ni_3Al (Ref. 18). Boron concentrations up to 1000 ppm have been shown to affect the room temperature mechanical properties of Ni_3Al (Ref. 22) as well as its weldability (Ref. 23). The materials used in the present study were selected so that the effect of boron on the weldability of Ni_3Al containing 10 at.-% Fe could be studied. The compositions of these two alloys were identical except for boron concentration: IC-25 contains 500 ppm B, while IC-103 contains only 200 ppm B. Therefore, Fig. 4 shows that welding speed and boron concentration both affect the weldability of Ni_3Al containing 10 at.-% iron.

Some insight into the effect of welding speed on weldability can be obtained by considering the effect of this variable on the thermal cycles experienced by a weldment (Refs. 26–28). High welding speeds produce very high heating and cooling rates, which in turn create very steep thermal stress gradients in the fusion zone and HAZ. The rapid thermal cycles also reduce the time available for thermally activated processes to occur. Evidence of the latter point can be seen by considering the effect of welding speed on β formation in weldments. At low welding speed, the temperature gradients in the HAZ normal to the fusion line are relatively flat and change slowly with time, while the opposite is true at high welding speed. This means that, if solid-state phase transformations are predicted at elevated temperatures, they will be more likely to occur at low welding speeds because the kinetic conditions will be relatively favorable. Examination of Figs. 5 and 7 shows this to be the case for IC-25 and IC-103. Above about 1250°C, the equilibrium diagram predicts the formation of β phase. However, β (actually β') was observed on HAZ grain boundaries only at low welding speeds. At the higher speeds, the effective time above the β phase solvus was not enough to permit β formation. In the fusion zone, the effect of welding speed was the opposite of that observed in the HAZ. High welding speeds resulted in more β phase being retained in the fusion zone at room temperature than was retained at low speeds. Apparently, the rapid cooling conditions following solidification permitted less β to dissolve during cooling. The formation of β phase, however, did not appear to be a major factor in the HAZ cracking observed in IC-25.

With regard to thermal stresses, high welding speeds tend not only to localize stresses due to the steep thermal gradients in the HAZ, but also to produce stress distributions that change rapidly with time (Refs. 27, 28). Thermal stress analyses (Refs. 27, 28) indicate that for a point in the HAZ close to the fusion line, longitudinal compressive stresses build up as the arc approaches and then reverse to become tensile in nature after the arc has passed. These tensile stresses may be high enough to exceed the local yield point of a material (Refs. 27, 28). The orientation of HAZ cracks in high-speed EB welds of IC-25 suggests that they were produced by longitudinal stresses such as those just described. Lack of evidence for liquid intrusion into the HAZ cracks in IC-25 indicates that the cracks occurred after passage of the molten weld pool at a time when material in the HAZ would have been in a state of tension. Because these Ni_3Al alloys have very good ductility below about 600°C, it is presumed that the HAZ cracks formed between 600°C and the solidus temperature. The intergranular nature of the cracking (Fig. 8C) indicates a weakening of the HAZ grain boundaries at elevated temperatures (Ref. 22). Because IC-103 did not experience HAZ cracking, even at high welding speeds, it may be concluded that this alloy, having good ductility at 1200° and 1250°C, could sustain higher levels of welding-generated thermal stress than could IC-25 without local HAZ fracturing.

Because both alloys had identical composition, except for boron concentration,

Table 2—Comparison of Ductility Data at 1200°C

Alloy	Boron Concentration (at.-%)	Location on Thermal Cycle	Tensile Elongation (%)
IC-25	0.24	Heating	0.0
IC-103	0.10	Heating	16.1

and both had base metal grain size of about ASTM 8, the weldability results suggest that boron was responsible for the observed behavior. More specifically, comparison of the high-speed weldment fracture surfaces shown in Figs. 8C and 8D suggests that the higher boron level of IC-25 may have adversely affected grain boundary cohesion in this alloy at high temperatures. Previous efforts to characterize directly the effect of thermal cycling on HAZ grain boundary boron concentrations have been inconclusive (Ref. 29). Therefore, hot ductility testing was undertaken to aid our understanding of the mechanical behavior of IC-25 and IC-103 at high temperatures.

The results for hot ductility testing of IC-25 and IC-103 (Figs. 10, 11) indicate a significant difference for testing of these alloys on the heating portion of the HAZ thermal cycle. An insight into this difference can be gained by examination of Figs. 12 and 14, which show, respectively, the fracture appearance of IC-25 and IC-103 ductility specimens tested at 1200°C, and the data presented in Table 2. These data show that IC-25 fractured in a completely brittle manner by intergranular failure with no ductility, while IC-103 exhibited considerable tensile elongation. The dislocation pile-up model developed by Liu and Inouye (Refs. 30, 31) may be used to analyze those observations. This model predicts

$$\epsilon_f = (\sigma_o - \sigma_i)/k + (\sigma_c k)\,(s/d)^{1/2}$$

where ϵ_f = fracture strain, σ_o = frictional stress opposing dislocation motion on slip planes, k and σ_i = material constants, d = grain size, s = distance beyond the tip of a dislocation pile-up, and σ_c = cohesive strength of grain boundaries.

The constants k and σ_i are mainly temperature dependent, and it is reasonable to assume that σ_o would be the same for IC-25 and IC-103. Therefore, this model predicts that, for a given test condition and constant grain size, ϵ_f increases with σ_c. Because the fracture strain of IC-103 is much larger than that of IC-25, this analysis suggests that the grain boundary cohesive strength of IC-103 is much higher than that of IC-25. This, in turn, indicates that the effect of boron on the ductility of these Ni-Fe aluminides at high temperature is the opposite of its effect at room temperature. The alloy with the lower boron concentration had better high temperature ductility.

If σ_c is lower than the yield strength of a material, σ_y, failure should occur by intergranular fracture without appreciable ductility. Apparently, this is the case for IC-25 at all temperatures above 800°C, and for IC-103 between 800° and 1200°C. On the other hand, when σ_c exceeds σ_y, plastic deformation should occur without intergranular fracture. This appeared to be the case for IC-103 tested at 1200° and 1250°C. Furthermore, when ϵ_f is larger than the critical strain required to nucleate recrystallization, and sufficient thermal activation exists, recrystallization should occur. This was also observed in iC-103.

Comparison of the data for tests on heating and cooling shown in Figs. 10 and 11 indicates that β phase formation reduced the ductility of IC-25 and IC-103 at all temperatures where significant ductility was recorded. This effect was particularly dramatic in IC-103 tested at 1200°C. The formation of β phase in the HAZ did not, however, appear to affect weldability. Since β (or β') phase was only observed at lower welding speeds, where neither alloy showed HAZ cracking, it is considered that the severity of thermal stress gradients was the more important factor in the cracking tendency.

Heat-affected zone cracking was only observed in IC-25 at high welding speeds. Since HAZ β phase was absent under these welding conditions, and the orientation of the cracks suggested that they were caused by tensile stresses, it is concluded that the on-heating tension tests correlated reasonably well with the observations on weldability. Analysis of cracked welds suggested that HAZ cracking in IC-25 resulted from grain boundary weakness at elevated temperatures. Analysis of the hot-ductility results confirmed that the grain boundary cohesive strength of IC-25 was lower than its yield strength above 800°C. The grain boundary strength of IC-103 was found to be higher than that of IC-25 at high temperatures, and the moderate ductility shown by IC-103 at 1200° and 1250°C appeared sufficient to prevent HAZ cracking in this alloy. A more detailed microstructural characterization and measurement of high temperature strength would be likely to lead to a detailed formulation of the HAZ cracking mechanisms in the Ni-Fe aluminides. These avenues, unfortunately, are beyond our capabilities at present.

The appearance of specimens fractured at 1300°C (Fig. 16) suggests that grain boundary liquation can occur in these alloys. Nevertheless, this phenomenon was not a factor in cracking tendency for the present experiments.

Summary

The weldability of Ni_3Al containing 10 at.-% Fe was found to be affected by welding speed and a small change in bulk boron concentration. At welding speeds below 13 mm/s, defect-free autogenous electron beam welds were made in both alloys used for this study. Above 13 mm/s, IC-25 (500 ppm B) displayed a strong tendency for HAZ cracking, while IC-103 (200 ppm B) did not. Examination of weldment microstructures suggested that the HAZ cracking in IC-25 resulted from thermal stresses imposed on this region of the weldments at elevated temperature, and was caused by grain boundary weakness.

Hot ductility testing showed that these aluminides generally had poor high temperature ductility. IC-25 had no significant ductility above 800°C, either on the heating or the cooling portion of the thermal cycle used for testing. IC-103 did show some ductility when tested on heating at 1200° and 1250°C. Analysis of the ductility data by use of dislocation pile-up model suggested that the grain boundary cohesive strength of IC-103 was higher than that of IC-25 at high temperatures. It may be concluded from this that the higher boron concentration of IC-25 degraded its elevated temperature ductility. The hot ductility data, therefore, correlated very well with the weldability observations in indicating that grain boundary weakness at elevated temperatures was responsible for the observed HAZ cracking.

Acknowledgments

The authors are grateful to R. A. Bradley and A. C. Schaffhauser for programmatic guidance, to J. D. Hudson and B. C. Leslie for technical assistance, and to Kathy Gardner for preparing the manuscript. Also, we wish to thank C. T. Liu and R. W. Swindeman for technical review of the manuscript. Research was sponsored jointly by the U.S. Department of Energy AR&TD Fossil Energy Materials Program and the Office of Energy Systems Research, Division of Energy Conversion and Utilization Technologies (ECUT) Program, under contract DE-AC05-84OR21400 with Martin Marietta Energy Systems, Inc.

References

1. Hansen, M. 1958. *Constitution of Binary Alloys.* p. 19, McGraw-Hill Book Company, New York, N.Y.

2. Elliot, R. P. 1965. *Constitution of Binary Alloys, First Supplement.* p. 48, McGraw-Hill Book Company, New York, N.Y.

3. Guard, R. W., and Westbrook, J. H. 1959. *Trans. AIME* 215:807-814.

4. Ochiai, S., Oya, Y., and Suzuki, T. 1984. *Acta Metall.*, 30:289-298.

5. Aitken, E. A. 1967. *Intermetallic Compounds.* J. H. Westbrook, ed., pp. 491-515, John Wiley and Sons, Inc., New York, N.Y.

6. Liu, C. T., and Koch, C. C. 1983. *Technical Aspects of Critical Materials Used by the Steel Industry,* Vol. IIB. NBSIR 83-2679-2, National Bureau of Standards.

7. Liu, C. T., and Stiegler, J. O. November 1984. *Science* 226:636-642.

8. Westbrook, J. H. 1957. *Trans. AIME* 209:898.

9. Seybolt, A. V., and Westbrook, J. H. 1964. *Acta Metall.* 12:449.

10. Aoki, K., and Izumi, O. 1970. *Nippon Kinzoku Gakkaishi* 41:170.
11. Grala, E. M. 1978. *Mechanical Properties of Intermetallic Compounds.* J. H. Westbrook, ed., p. 358, John Wiley and Sons, Inc., New York, N.Y.
12. Moskovic, R. 1978. *J. Mater. Sci.* 13: 1901.
13. Aoki, K., and Izumi, O. 1978. *Trans. JIM* 19:203.
14. White, C. L., and Stein, D. F. 1978. *Metall. Trans. A* 9A, p. 13.
15. Ogura, T., Hanada, S., Masumoto, T., and Izumi, O. 1985. *Met. Trans. A* 16A, pp. 441-443.
16. Aoki, K., and Izumi, O. 1979. *Nippon Kinzoku Gakkaishi* 43:1190.
17. Liu, C. T., *et al.* 1983. *Proc. Symp. High Temperature Materials Chemistry II.* Mumir, *et al.*, ed., The Electrochemical Soc., Inc.
18. Liu, C. T., *et al.* August 1984. *Initial Development of Nickel and Nickel-Iron Aluminides for Structural Uses,* ORNL-6067.
19. Liu, C. T. 1984. *Int. Met. Rev.* 29 (3):168-194.
20. Briant, C. L., and Messmer, R. P. 1980. *Phil. Mag. B* 42:567.
21. Messmer, R. P., and Briant, C. L. 1982. *Acta Metall.* 30:457.
22. Liu, C. T., White, C. L., and Horton, J. A. 1985. *Acta Metall.* 33(2):213-229.
23. David, S. A., *et. al.* 1985. *Welding Journal* 64(1):22-s to 28-s.
24. Rosen, S., and Goebel, J. A. 1968. *Trans. AIME* 242:722-724.
25. Moskovic, R. 1977. *J. Materials Sci.* 12: 489-493.
26. Yeniscavich, W. 1970 *Proceedings of a Symposium on Methods of High-Alloy Weldability Evaluation.* Welding Research Council p. 2.
27. Masubuchi, K. 1980. *Analysis of Welded Structures,* Pergamon Press Ltd.
28. Kou, S., and Lee, Y. 1983. *Met. Trans. A* 14A, p. 2245.
29. Santella, M. L., and David, S. A. *Proceedings of a Symposium on High-Temperature Ordered Intermetallic Alloys, November 1984.* Materials Research Society, 1985. To be published.
30. Liu, C. T., and Inouye, H. 1976. *Proceedings of the 2nd International Conference on the Mechanical Behavior of Material.* ASM, pp. 1149-1153.
31. Liu, C. T., Inouye, H., and Schaffhauser, A. C. 1981. *Met. Trans. A* 12A, pp. 993-1002.